Colloids and Surfaces B: Biointerfaces 146 (2016) 39–46

Contents lists available at ScienceDirect

Colloids and Surfaces B: Biointerfaces

journal homepage: www.elsevier.com/locate/colsurfb

Nanomaterial resistant microorganism mediated reduction of graphene oxide

Raghuraj S. Chouhan, Ashish Pandey, Anjum Qureshi, Volkan Ozguz, Javed H. Niazi*

Sabanci University Nanotechnology Research and Application Center, Orta Mah., 34956 Istanbul, Turkey

ARTICLE INFO

Article history:
Received 12 February 2016
Received in revised form 14 April 2016
Accepted 17 May 2016
Available online 18 May 2016

Keywords:
Graphene oxide
Biotransformation
Resistant bacteria
Nanomaterials

ABSTRACT

In this study, soil bacteria were isolated from nanomaterials (NMs) contaminated pond soil and enriched in the presence of graphene oxide (GO) in mineral medium to obtain NMs resistant bacteria. The isolated resistant bacteria were biochemically and genetically identified as *Fontibacillus aquaticus*. The resistant bacteria were allowed to interact with engineered GO in order to study the biotransformation in GO structure. Raman spectra of GO extracted from culture medium revealed decreased intensity ratio of I_D/I_G with subsequent reduction of C=O which was consistent with Fourier transform infrared (FTIR) results. The structural changes and exfoliatied GO nanosheets were also evident from transmission electron microscopy (TEM) images. Ultraviolet–visible spectroscopy, high resolution X-ray diffraction (XRD) and current-voltage measurements confirmed the reduction of GO after the interaction with resistant bacteria. X-ray photoelectron spectroscopy (XPS) analysis of biotransformed GO revealed reduction of oxygen-containing species on the surface of nanosheets. Our results demonstrated that the presented method is an environment friendly, cost effective, simple and based on green approaches for the reduction of GO using NMs resistant bacteria.

1. Introduction

The unique physiochemical properties of carbon nanostructured graphene [1] showed high impact applications in materials [2–5] and biomedical sciences [6–12]. Highly promising and novel applications of graphene (Gr) resulted in increasing requests for mass production of graphene oxide (GO). Several techniques to prepare high quality graphene, aerographite and related nanomaterials have been reported, such as micromechanical exfoliation by scotch tape, epitaxial growth on electrically insulating surfaces like, silicon carbide and chemical vapor deposition onto thin films or networks of metal [13,14]. All these methods can synthesize high quality of Gr, but finds limitations for mass production [13,15]. In this regard, chemical oxidation and subsequently exfoliation of graphite oxide is used as a common method for synthesis of GO sheets, which requires a subsequent reduction process for converting into Gr. The reduction of GO to Gr is accomplished by using biologically harmful chemical reducing reagents, such as anhydrous hydrazine, hydrazine monohydrate, sodium borohydride, hydrogen sulfide, flash photolysis, microwave irradiation, thermal shock, photo-catalytic degradation and catalytic reduction in the liquid phase [2,13]. Additionally, the chemical oxidation–reduction methods also suffer from being environmentally harmful approaches with limitations for mass production of GO/Gr sheets. Therefore, it is imperative to develop alternative eco-friendly approaches for reduction/oxidation of carbon nanostructures that are not only safe but also inexpensive for large-scale synthesis.

Recently, researchers have reported eco- friendly methods for the production of chemically/biologically reduced GO. For example, Salas et al. have studied "green" reduction of GO by bacterial respiration involving membrane proteins that are originally responsible for metal reduction [16]. Biologically useful chemical, ascorbic acid and living bacteria, such as *Shewanella* sp. have also been used for the reduction of GO to Gr [17,18] . Further, Akhavan and Ghaderi investigated interactions between exfoliated GO sheets and *Escherichia coli* bacteria under anaerobic conditions in which the GO sheets served as biocompatible sites for adsorption and proliferation of the bacteria on their surfaces [19]. Such interactions are primarily responsible for triggering biological reactions between metal-reducing membrane proteins and the interacting carbon nanostructures [16]. Environment-friendly chemical agents other than vitamin C [17], such as aluminum powder, reducing sug-

* Corresponding author.
E-mail address: javed@sabanciuniv.edu (J.H. Niazi).

http://dx.doi.org/10.1016/j.colsurfb.2016.05.053
0927-7765/

ars and amino acids have been used to produce reduced GO [20–22]. Wang et al. demonstrated that microbial reduction of GO occurs in a normal aerobic cultural set-up using *Shewanella* cells and that anaerobic conditions are not essentially required for GO reduction [23]. Similarly, *E. coli* cells have also been used for the microbial reduction of GO under aerobic conditions [24]. Tanizawa et al. developed a hybrid approach for the synthesis of reduced Gr sheets from chemically derived GO using aerobic microorganisms isolated from river sediments [25]. All the above GO reduction methods are promising alternatives for green synthesis of Gr that are currently in developmental stages and requires extensive investigation.

Researchers are interested to explore various green approaches for synthesizing Gr in commercial quantities. Therefore, it is highly desirable to develop new strategies for large-scale GO reduction under mild and environmentally compassionate conditions. Thus, it is imperative to explore the possibility of NMs reduction/oxidation mainly by the action of microbes or at cellular levels. Evolutionary process for microorganisms to naturally adapt to NMs is a relatively slow process, which may last decades. Therefore, reduction of carbon based NMs by microorganisms is virtually an unexplored area. Reducing NMs by microorganisms is an effective means to "green nanotechnology" This process required external carbon source involving co-metabolism and the cooperation of several microbial consortia. However, a structural transformation in NMs during the bacterial degradation/reduction/oxidation process is still unclear. The accelerated transport of metal oxide nanoparticles were observed in soil and river samples collected from Germany and Sweden [26,27]. The soil samples from these sites are found to be NMs contaminated, and bacteria isolated from these samples may acquire resistance against NMs. Therefore, we developed a simple and green approach in which microorganisms isolated from NMs contaminated pond site were employed for biotransformation of GO nanostructure. The isolated microorganisms were tuned to evolve or adapt rapidly against NMs in the laboratory, through repeatedly exposing them to NMs under controlled conditions, such as by providing essential nutrients, minerals and experimentally defined physical factors. A combination of the above processes enabled isolating resistant microorganisms with new or alternative transformation pathways that resulted in partial biological reduction of GO nanostructure.

2. Material and methods

2.1. Reagents and chemicals

Engineered GO (<4 layers; 1–15 nm/5 nm Thickness; Surface area 700 m^2/g; 2 μm diameters) was purchased from Carbon Solutions Inc., USA. Dimethyl Sulfoxide (DMSO), KH_2PO_4, Na_2HPO_4, NH_4Cl, NaCl, $MgSO_4$, Tryptic soya broth (TSB) were purchased from Sigma-Aldrich, USA. All other reagents used in this study were of analytical grade and filtered through 0.22 μm sterile filters.

2.2. Collection of soil sample, preservation and storage

Soil samples were collected from pond side near Kiel, Germany (Temperature: 20–27 °C; Latitude−54°19′31.2456″; longitude−10°8′3.6522″). The collected soil samples were appropriately labelled and transported to the laboratory using Standard Operating Procedures (SOPs). The collected soil samples were homogenized in a container constructed of inert material and transferred to appropriate sample medium for the propagation of soil bacteria.

2.3. Isolation and enrichment of soil bacteria to obtain GO resistant bacteria

Soil samples (25 g each) were suspended in basal mineral medium (MM) separately and diluted appropriately and filtered through a column with a glass-wool plug to remove undesirable suspended particles from the soil. The basal MM (per litre) contained 3 g KH_2PO_4, 12.8 g $Na_2HPO_4{\cdot}7H_2O$, 1 g NH_4Cl, 0.5 g NaCl and supplement sources such as $MgSO_4$ (2 mM), $CaCl_2$ (0.1 mM) and glucose (varying from 0.3–0.4%). The pH (6.5–7.5) of basal MM and the temperature (25–37 °C) was varied depending upon the growth requirements of the soil microbial flora and modified by removing specific salts accompanied by supplementing with different carbon/nitrogen sources (e.g., NH_4NO_3 in place of NH_4Cl). Alternatively, resistant bacteria were also grown in TSB medium for rapid screening of mixed bacterial colony characteristics. The TSB medium contained (per litre) 17 g Tryptone (pancreatic digest of casein), 3 g Soytone, 2.5 g dextrose, 5 g Sodium chloride and 2.5 g K_2HPO_4, pH 7.3. Cultures grown on basal MM were only considered for enrichment while cultures grown in nutrient rich TSB medium were used only for screening colony characteristics because of the possibilities of losing the ability of bacterial adaptation to GO. Culture flasks that showed good growth in MM were amended with GO. GO suspension was prepared in PBS pH-7.4 and homogenized using probe ultrasonicator for 15 min. The homogeneous stock suspension of GO (5–15 μg/mL) was prepared freshly prior to the start of the experiment. To avoid the undesirable growth of contaminating fungi in cultures, >0.5 μg/mL of cycloheximide (an anti-fungal agent) was added into the medium before inoculation for three subsequent subcultures and withdrawn when all of the fungi were eliminated. Initially, 5 μg/mL GO was amended in the media to interact with the soil bacteria and incubated the flasks at 25–37 °C at 125 rpm for over two years and replenished with fresh medium every 60 days interval for over 14 months. Depending upon the resistance of bacteria, GO concentration was increased to 15 μg/mL and this concentration was maintained throughout the enrichment process. Thus obtained resistant bacterial species were isolated and utilized for characterization.

2.4. Biochemical characteristics of isolated GO resistant bacteria

In this study, standard biochemical tests that are commonly used (listed in Table S1) for bacterial identification were applied for identification of isolated NM-resistant bacteria. Fresh colonies from all the isolated samples were selected and grown in MM agar containing 0.4% glucose for 48 h. Pure bacterial colonies from the MM agar plates were picked, suspended in sterile saline solution and vortexed. Each sample was assigned a unique identity to avoid confusion for interpretation of final results. A total of 21 biochemical tests were carried out for the identification of bacteria and the results were interpreted using an online chart (http://faculty.ivytech.edu/~bsipe/UNKN/ukkey.htm) according to Bergey's Manual of Systematic Bacteriology. All biochemical tests that were carried out are listed in Table S2 using standard commercial biochemical kits (Analytab Products, Inc.).

2.5. Identification of GO resistant bacteria by genetic method

Genomic DNA from the GO-resistant bacteria was extracted and purified using a Qiagen DNA extraction kit and used as template for amplifying the 27f–1492r regions of the 16S rDNA by PCR using the following universal primer pairs; forward (27f) 5′- AGAGTTTGATCCTGGCTCAG-3′ and reverse (1492r) 5′-TACCTTGTTACGACTT- 3′. Each PCR reaction mixture contained 25 μL of premix Taq (TaqMix, Qiagen), 100 nM of each primer (27f and 1492r), 1 μL of template DNA (genomic DNA extracted from

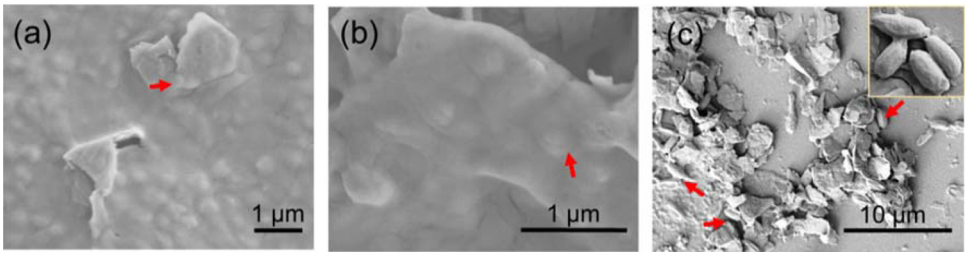

Fig. 1. SEM images of culture residue showing the GO resistant bacteria and their aggregation with GO. (a and b) SEM images of bacterial cells and GO aggregates at different magnifications showing a thick blanket-like structure of a slimy layer formed over the GO nanosheets. (c) Individual cells interacting with nanosheets are highlighted with red arrows. The inset image in (c) is the enlarged portion of a section showing intact morphology of bacterial cells. (For interpretation of the references to colour in this figure legend, the reader is referred to the web version of this article.)

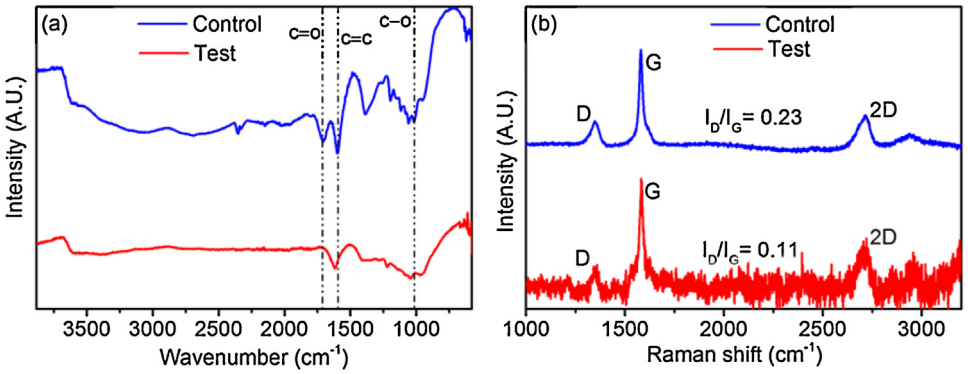

Fig. 2. (a) Fourier transform infrared spectra and (b) Raman spectra of graphene oxide extracted from the control (in absence of bacteria) and test (in presence of resistant bacteria) culture medium.

resistant bacteria), and the total reaction volume finally adjusted to 50 μL with sterile distilled H_2O. For PCR amplification, following optimized conditions were applied; (i) initial DNA denaturation at 94 °C for 5 min, (ii) 32 cycles of DNA denaturation at 94 °C for 1 min, annealing at 55 °C for 1 min, and amplify at 72 °C for 1 min and (iii) final extension step at 72 °C for 10 min. About 5 μL of the amplified PCR products thus obtained was resolved on 1% agarose by gel electrophoresis and confirmed the expected PCR product size of 1465 bp. The pure PCR product of 1465 bp size was purified and sequenced. The raw unprocessed sequencing data was directly applied for genetic identification of bacteria by clustering and phylogenetic analysis using BIBI Database (http://pbil.univ-lyon1.fr/bibi/). The BIBI tool enabled identifying the type of bacteria based on its 16S rDNA sequences using BLAST and the phylogenetic analysis was performed using ClustalW2 program. Thus obtained results were analyzed on the basis of sequence composition, information from BLAST and phylogenetic reconstruction on quality of the sequence query and compared the node distances for many sequence clusters from various other related species.

2.6. Interaction and extraction of engineered GO

25 mL of GO resistant bacterial cultures grown for at least 30-days in presence of GO in MM were separated by centrifugation at 9000 rpm for 10 min and the supernatant was discarded. The pellet containing GO, cells and cell-debris was washed thrice with pure ethanol and sonicated for 15 min and centrifuged to separate the cells and cell-debris. The supernatant containing cell debris was discarded and the brownish pellet containing GO was phase separated in a mixture of 1:1 *N*-hexane:deionized water and centrifuged at 9000 rpm for 5 min. A brownish coloured ring of purified GO appeared at the interface of two solvent phases. Finally, pure GO was carefully collected in a separate glass vial, washed with deionized water and dried in vacuum desiccator before the sample was used for further characterizations.

2.7. Characterizations

2.7.1. Scanning electron microscopy (SEM) analysis

The bacteria-GO aggregates from the culture medium were directly filtered through a column with a glass-wool plug. The filtrate residue was washed with phosphate buffered saline (PBS) pH 7.4 and the residue was then mounted on a silicon wafer, dried and sputter coated with a thin layer of Pd–Au before taking SEM images. SEM images were acquired using a LEO Supra 35VP scanning electron microscope operated at 3 kV.

2.7.2. TEM analysis

The extracted pure GO from the culture medium was re-suspended in deionized water. A drop of this suspension was placed directly on Lacy Carbon Type-A 300 mesh copper grids (Ted Pella, USA). The suspension was drawn through the grid by placing a lint-free tissue under the grid and dried. To reduce the formation of salts on the TEM grid, the grids were briefly washed with a droplet of water and allowed to dry before imaging. TEM images were acquired using a JEOL JEM-ARM200CFEG UHR equipped with a CCD camera and operated at an acceleration voltage of 100 kV.

2.7.3. Raman, FTIR and ultraviolet–visible (UV–vis) spectra

Raman spectra of control (engineered GO before interaction of resistant bacteria) and test (GO after interaction of resistant bacteria) GO samples were measured using Renishaw inVia Reflex Raman Microscope and Spectrometer (visible excitation at 532 nm laser) with spectral resolution of 5 cm^{-1}. FTIR spectra were used to study characteristics of functional groups on control and test samples. FTIR spectra were acquired using a Nicolet iS10 FTIR Spectrometer

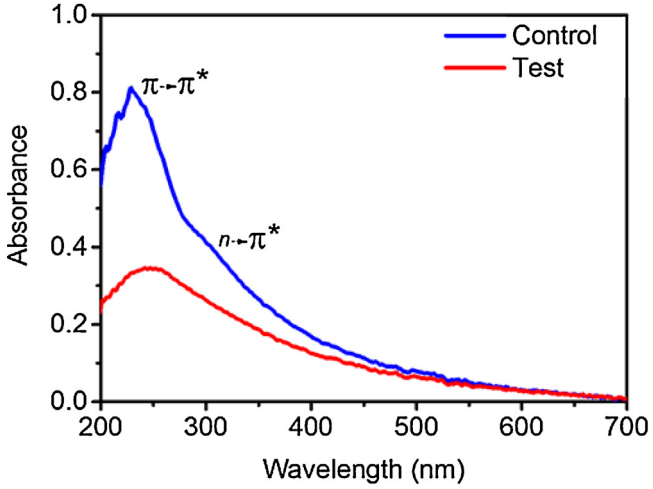

Fig. 3. UV–vis spectra of GO samples extracted from control culture medium (without bacteria) and test culture medium (with resistant bacteria). Control GO exhibited two absorption peaks at 230 and ~300 nm that corresponds to the π-π* transition of the C—C bonds and n → π* transition of the C═O bonds, respectively. The plasmon peak shift in test GO at 250 nm is attributed to possible reduction of GO due to biocatalytic action of nanomaterial resistant bacteria.

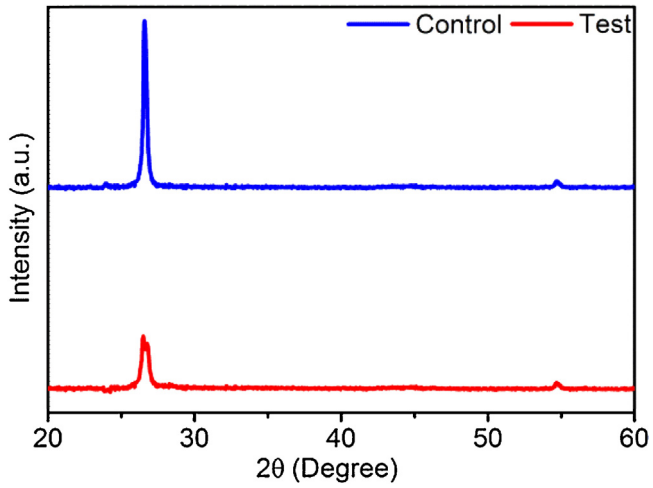

Fig. 4. X-ray diffraction patterns of GO samples extracted from control culture medium (in absence of bacteria) and test culture medium (in presence of resistant bacteria). The XRD pattern of test GO sample showed reduced graphitic peak intensity relative to control.

(Thermo Scientific, USA) with mercury cadmium telluride detector (4 cm^{-1} resolution). IR spectra of sample mounted on silicon wafer were collected with an average of 100 scans with a wide spectral range from 300 to 4000 cm^{-1}. UV–vis spectra were obtained using NanoDrop 2000 spectrophotometer (Thermo Scientific, USA).

2.7.4. X-ray diffraction

The dried extracted sample of GO (control and test) were placed on glass slides followed by a drop of ethanol and dried. These glass slides were then placed on the sample holder and the X-ray diffraction analyses were carried out using Bruker D8 DISCOVER X-ray diffractometer (Bruker AXS GmBH, Karlsruhe, Germany). High resolution XRD patterns of samples were measured at 3 Kw with Cu target using scintillation counter (λ = 1.5406 Å) at 40 kV in the range of 2θ = 2–90°.

2.7.5. Current-Voltage (I–V) measurements

I–V curves of the GO sheets extracted from the culture medium in absence (control) or presence of resistant bacteria (test) were

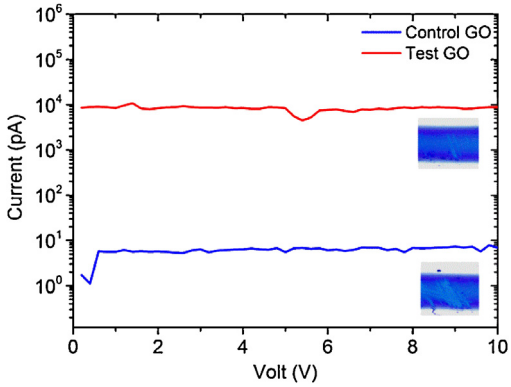

Fig. 5. Current-voltage characteristics of GO samples extracted from control culture medium (without bacteria) and test culture medium (in presence of resistant bacteria). The inset images show respective GO nanosheets casted between the gold electrodes.

measured using a Keithley 6571B electrometer. For this measurement, the extracted GO sheets were drop-casted between the two Au electrodes that were previously patterned on the SiO_2/Si substrates. Then, the GO sheets deposited on the Au electrodes were dried and annealed at 200 °C in air for 30 min before taking *I–V* measurements.

2.7.6. XPS analysis

For XPS analysis, the control and test samples were mounted on a carbon tape and recorded the XPS spectra using a Thermo Scientific K-Alpha X-ray photoelectron spectrometer. Monochromatized Al Kα radiation (Al Kα = 146.3 eV) was used as the X-ray source and flood gun was used for charge compensation during the measurements. The X-ray spot size was approximately 400 μm. Electron take-off angle between the sample surface and the axis of the analyzer lens was set to 90°. Spectra were recorded using Avantage 5.9 data system. The binding energy scale was calibrated by assigning the C1s signal at 284.5 eV.

3. Results and discussions

3.1. Isolation and enrichment of bacteria to obtain NMs resistant bacteria

In this study, soil samples near pond sites that have a prior history of nanomaterial contamination were collected as a source of persistent bacteria capable of utilizing GO (Fig. S1). This allowed exploring potential nano-size-stress-resistance soil bacterial populations from pond site that have been found to contain metal oxide leachates with nano/micro particles or colloidal suspensions [26,27]. Metallic particle was detected in the form of micro precipitates on the biomass surfaces as well as in colloidal form as nano-particles in the solution [26,27]. These soil bacteria isolated from soil samples (pIA, pIB, pIC, pID and pIE) were incubated with GO for adaptation (Fig. S1). Each soil sample was suspended in the MM and divided into two pools for control and test flasks, respectively and screened for the influence of growth in presence of GO. Images of flasks that showed positive growth in presence of GO were documented for comparison with respective controls. The enriched soil microbial population was subjected to acclimatization (adaptation) to efficiently grow and resist against GO under artificially created environment in a climate chamber (Fig. S1).

The resistant bacterial population was subjected to screening and isolation of the most dominant bacterial candidate from the mixed population and examined using SEM images (Fig. 1). The resistant bacterial candidate showed adaptation with a high degree of survival and tolerance to GO. SEM image of isolated GO-resistant

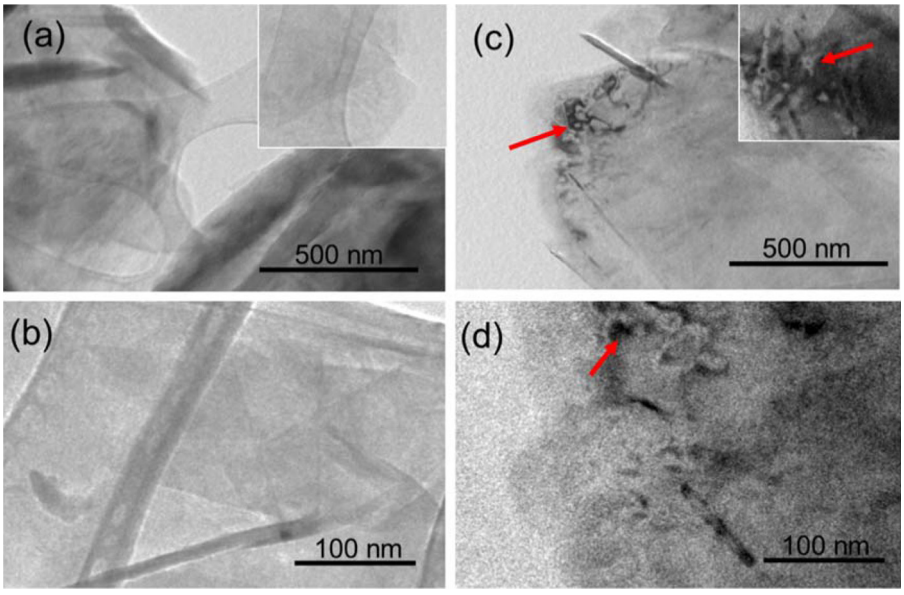

Fig. 6. High resolution TEM images of GO samples extracted from the culture medium at different magnifications. (a and b) TEM images of GO extracted from control medium in absence of resistant bacteria. (b and c) TEM images of GO extracted from test medium after their interaction with resistant bacteria. The inset image in (a) shows smooth edges with clear surface of GO nanosheet and the inset image in (b) show rough and exfoliated GO nanosheets with groves and ridges highlighted by red arrows. (For interpretation of the references to colour in this figure legend, the reader is referred to the web version of this article.)

bacteria showed secretion of a slimy by-product to protect the cells from rupturing with GO nanoplatelets (Fig. 1c-a). The isolated bacteria and GO aggregates formed a blanket of nanoplatelets sheath (Fig. 1c). Dispersed bacteria from the aggregates showed tight entrapment of GO around the cells where extracellular oxidative enzymes likely to be interacted (Fig. 1d).

3.2. Identification of GO resistant bacteria by biochemical and genetic methods

The biochemical tests enabled identifying different bacterial species as a result of various metabolic properties of bacterial cells. The results of biochemical tests to identify the GO-resistant bacteria were scored as "+" or "−" codes through color change or release of gases according to the standard protocol for each sample [28] (Table S1). Based on the screening of biochemical characteristics of sample, GO-resistant bacteria were aerobic (catalase positive) and exhibited negative carbohydrate fermentation tests indicating non-fermenting nature of bacteria (Tables S1 and S2). These test results in combination with others including Gram staining enabled identifying as Gram negative bacteria which was rod shaped in structure. The enriched bacterium was subjected to genetic identification using 16S rRNA sequencing followed by phylogenetic analysis (Fig. S2). The results showed that the GO-resistant bacteria was *F. aquaticus* which is mainly found in dusts or soil [29].

3.3. Physico-chemcial analysis of GO extracted from the culture medium

3.3.1. FTIR and Raman spectroscopy analysis

GO was first extracted from the culture medium after its interaction with resistant bacteria (test). GO without any interaction with resistant bacteria under identical conditions served as a control. The samples were subjected to FTIR and Raman spectroscopy analysis and the results are shown in Fig. 2a and b. The FTIR spectra of control GO showed a strong and broad absorption at 3400 cm^{-1} due to the O—H stretching vibration (Fig. 2a). The C=O stretching peak was observed at 1730 cm^{-1} and the peak at 1620 cm^{-1} may be attributed to C=C stretching vibration of carbon skeleton vibrations in control sample. The peak at 1400 cm^{-1} may be assigned to tertiary C—OH groups. The peak at 1216 cm^{-1} represents stretching of C—O—C and the peak at 1082 cm^{-1} corresponds to C—O groups [30,31] (Fig. 2a). The diminishing of C=O at 1730 cm^{-1} was observed in GO test sample upon interaction with resistant bacteria (Fig. 2a). The intensity of the broad band at 3400 cm^{-1} decreased and the changes suggested that most of the hydroxyls and carbonyls were degenerated from the surface of a few layers of test GO sample. These results suggested that GO structure interacted with the resistant bacteria which reduced the accessible GO surface through possible biocatalytic mechanism. These mechanisms are often mediated by the intracellular or extracellular redox enzymes that reduce or oxidize substrates available in their surroundings (enzymatic catalysis). Studies on enzymatic catalysis mainly by horseradish peroxidases and myeloperoxidases have been reported to partially degrade CNTs through biocatalytic oxidations [32–35]. Similar type of reduction of GO has been reported after its interaction with Lawesson's reagent (LR) and strong acids [36,37] .

Raman spectral analysis of GO extracted from the culture medium after its interaction with resistant bacteria revealed the partial biodegradation of GO (Fig. 2b). The intensity ratio of D (~1350 cm^{-1}) and G (~1580 cm^{-1}) (I_D/I_G) were considered to analyse the biotransformation/biodegradation of test GO in comparison to control. After interaction of GO with resistant bacteria (test), the GO structure showed significant spectral modifications as shown in Fig. 2b. The shortening of the D and G bands were observed in GO test sample as compared to control implies partial exfoliation/degradation of GO structure, suggesting the efficiency of bacteria in biotransforming GO by exfoliating a few layers. The ratio of I_D/I_G with test GO (0.11) decreased as compared to control GO (0.23) sample (Fig. 2b). This change in ratio indicated the structural variations induced by the bacterial catalysis and thus, structural transformations of a few layers of GO. It also implied that NM-resistant *F. aquaticus* created more disintegration of the multiple stacked layers of graphene due to their respiration process similar to that reported previously [16]. Comparison of Raman and FTIR spectra of GO test samples clearly indicated that the GO layers were structurally degraded through possible surface reduction due to their interaction with resistant bacteria.

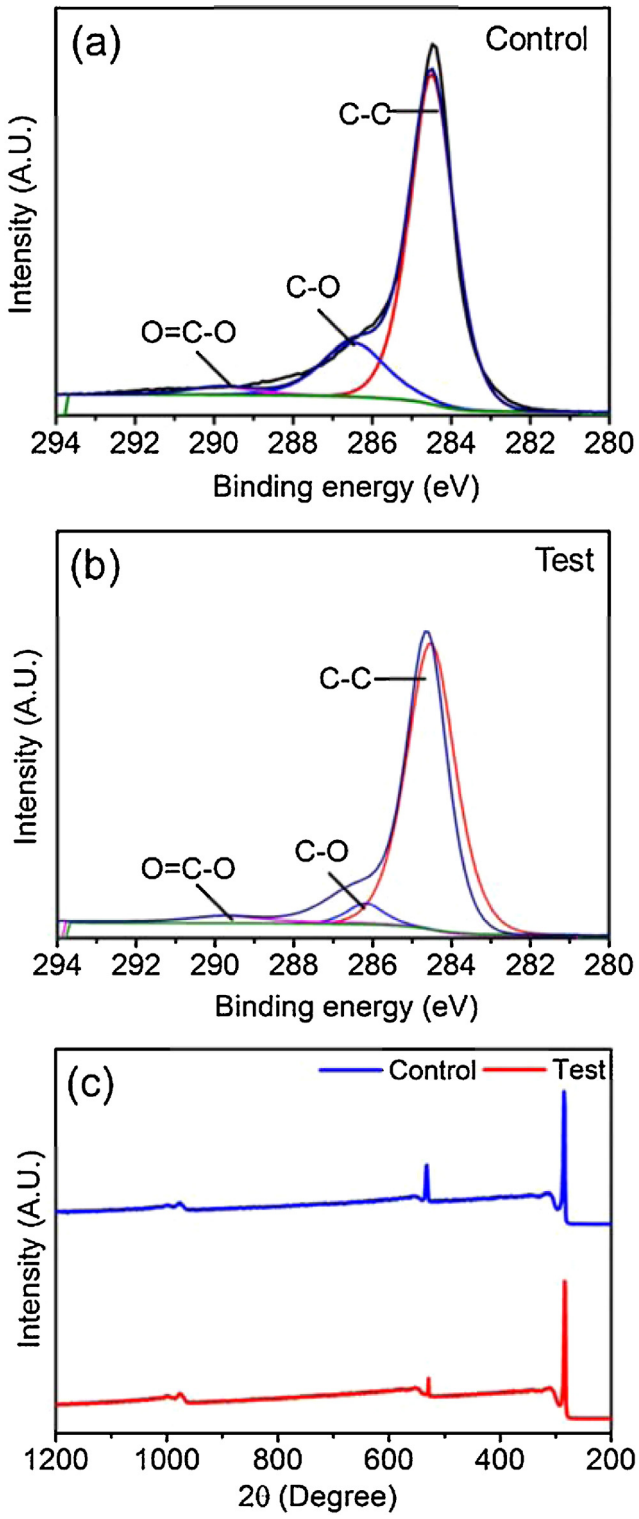

Fig. 7. XPS spectra of the C1s of GO extracted from; (a) control medium in absence of resistant bacteria, (b) test medium after the interaction with resistant bacteria and (c) survey spectra of both test and control GO samples.

3.3.2. UV–visible spectroscopy

The UV–vis absorption spectra showed that control GO exhibited two absorption peaks at 230 nm and 300 nm. The peak at 230 nm corresponds to π-π* transition of the C—C bonds and a shoulder peak at ~300 nm corresponds to the n → π* transition of the C=O bonds (Fig. 3) [24] . However, test GO showed the plasmon peak gradually shifted at 250 nm after possible reduction process occurred due to biocatalytic action of NM-resistant bacteria. The shift towards higher absorption band suggested that electronic transitions/conjugation occurred in test GO nanostructure after resistant bacteria mediated reduction of nanosheets [38,39]. The absorption in spectral region (>230 nm) in test GO showed broader absorption peak area as compared with control GO, which indicates the restoration of the π-π* conjugation within the graphene nanosheets (Fig. 3) [40]. Similar results were observed for the reduction of GO by L-ascorbic acid [41], L-cysteine [22], with the biomass of bacteria and baker's yeast [38,18,42].

3.3.3. XRD analysis

The XRD patterns of control and test GO are shown in Fig. 4. The XRD pattern of test GO sample showed reduced graphitic peak intensity as compared with the control GO sample (Fig. 4). This inferred that the conjugated graphene network (sp^2 carbon) seemed to re-establish the structure from GO during the reduction mechanism induced by the resistant bacteria. Such type of GO reduction is associated with the ring-opening of the epoxides [43]. The changes in test GO structure mediated by the bacterial reduction process were also reflected in the Raman spectra in which the I_D/I_G ratio decreased from 0.26 to 0.11 after the bacterial interaction (Fig. 2b). The ratio of I_G/I_D is proportional to the in-plane graphitic crystallite size [44], therefore our results suggested that the crystallite size of sp^2 domains in the graphene sheets partially degraded by the biocatalytic mechanisms of bacteria. The XRD peak intensity at $2\theta = 26^\circ$ was reduced in test GO as compared with control, suggesting the amorphous and exfoliated randomly packed structure of reduced GO sheets (Fig. 4).

3.3.4. Current-Voltage (I–V) characteristics

To confirm the reduction of the GO nanosheets extracted from the culture medium, the *I–V* characteristics were measured. The control (in absence of bacteria) and test GO samples (in presence of resistant bacteria) were deposited between Au electrodes and measured the current against the applied voltage. It was observed that the current density increased in test GO nanosheets after their interaction with resistant bacteria as compared with control GO nanosheets (Fig. 5). This result is consistent with previous reports on GO reduction by chemical, thermal and microbial processes [16,19,45,46]. Comparing the current density values with the ones reported earlier for GO, it is clear that the resistant bacteria mediated higher capacity of reduction in GO nanosheets [16].

3.3.5. TEM analysis

TEM image analysis was performed to characterize the structural changes in control and test GO extracted from the culture medium. The control GO nanosheets were flat and intact in their structure with smooth surface and uniformly arranged as multilayered sheets with no aggregates or defects (Fig. 6a and b). The GO nanosheets extracted from the test culture medium consistently showed several small patches of exfoliated sheets and cleavages of nanoribbon architecture (Fig. 6c and d, red arrows). Defects extending from the outer to inner layers of the GO sheets were also observed (Fig. 6c; inset picture). The results of TEM examination are in good agreement with those changes observed in FTIR and Raman spectra of same GO samples (test and control) that clearly showed deformation of functional groups on GO surface and their I_D/I_G ratios, respectively (Fig. 2a and b).

3.3.6. X-ray photoelectron spectroscopy

The changes in reduction level of extracted GO samples from control and test culture medium were also analysed by recording XPS spectra. Fig. 7a–c shows intensities of O1s and C1s spectral envelopes in test and control GO nanosheets. The C1s XPS spectra

of control and test GO nanosheets were resolved into different characteristic peaks. The peaks centred at binding energies of 284.5 eV, 286.3 eV and 289.2 eV were attributed to C—C, C—O and O=C—O, respectively corresponding to carbon atoms bonded with different oxygen groups [37,47]. As compared with C1s XPS spectra of control GO nanosheets (Fig. 7a), biotransformed GO nanosheets (test sample) displayed decrease in the intensity of O=C—O at 289.2 eV that revealed bacteria induced reduction of oxygen species (Fig. 7b). The decreased level of surface oxygen on the biotransformed GO layers was also confirmed from survey spectra (Fig. 7c). Interaction of resistant bacteria induced changes in the surface profile of GO after prolonged incubation which resulted in the biological reduction action on the nanosheets and subsequently enabled exfoliating of a few layers (Figs. 6 c and d and 7 a–c). The results of XPS analysis were in good agreement with FTIR and Raman spectra and therefore, the structural changes occurred on GO test samples were ascribed to the bacterial bio-catalytic activities to diminish functional groups on the surface of GO nanosheets (Fig. 2a and b). Our results are also consistent with those of chemical reduction processes reported previously by utilizing strong chemical agents for the synthesis of GO that effectively change the functional groups and arrangements of sp^2 lattice structure on GO surfaces [37,47].

4. Conclusion

In this study, we presented a unique green approach complementary to NM toxicological studies which utilized NM-resistant bacteria to mediate the reduction of GO. This NM-resistant bacteria was isolated after successive enrichment process in presence of engineered GO and identified biochemically and genetically as *F. aquaticus*. Raman spectra of biotransformed/reduced GO extracted from culture medium revealed decreased intensity ratio of I_D/I_G with subsequent reduction of C=O bonds. UV spectra, XRD and I–V characteristics results confirmed the reduction of GO by resistant bacteria. XPS analysis revealed reduction of oxygen- containing species on the surface of nanosheets after their interaction with resistant bacteria. The structural changes such as roughness, distortion and exfoliation upon interaction with NM resistant bacteria were also observed. Our results demonstrated that the biotransformation of GO were induced through reduction and exfoliation of GO nanosheets. The proposed approach has a potential to use selected NMs resistant bacteria for reduction of GO with new properties that are safe for industrial applications.

Acknowledgements

This work was support by the Scientific and Technological Research Council of Turkey (TUBITAK) to the author JHN with project grant No. 112Y309. We thank Dr. Barış Yağcı, Koç University Surface Science and Technology Center (KUYTAM) for performing XPS analysis.

Appendix A. Supplementary data

Supplementary data associated with this article can be found, in the online version, at http://dx.doi.org/10.1016/j.colsurfb.2016.05.053.

References

[1] H.-P. Boehm, Graphene-how a laboratory curiosity suddenly became extremely interesting, Angew. Chem. Int. Edn. 49 (2010) 9332–9335.
[2] A.K. Geim, K.S. Novoselov, The rise of graphene, Nat. Mater. 6 (2007) 183–191.
[3] X. Li, X. Wang, L. Zhang, S. Lee, H. Dai, Chemically derived, ultrasmooth graphene nanoribbon semiconductors, Science 319 (2008) 1229–1232.
[4] K.A. Ritter, J.W. Lyding, The influence of edge structure on the electronic properties of graphene quantum dots and nanoribbons, Nat. Mater. 8 (2009) 235–242.
[5] D.R. Kauffman, A. Star, Graphene versus carbon nanotubes for chemical sensor and fuel cell applications, Analyst 135 (2010) 2790.
[6] L. Feng, Z. Liu, Graphene in biomedicine: opportunities and challenges, Nanomedicine 6 (2011) 317–324.
[7] K. Yang, S. Zhang, G. Zhang, X. Sun, S.-T. Lee, Z. Liu, Graphene in mice: ultrahigh in vivo tumor uptake and efficient photothermal therapy, Nano Lett. 10 (2010) 3318–3323.
[8] B. Tian, C. Wang, S. Zhang, L. Feng, Z. Liu, Photothermally enhanced photodynamic therapy delivered by nano-graphene oxide, ACS Nano 5 (2011) 7000–7009.
[9] G. Lalwani, A.T. Kwaczala, S. Kanakia, S.C. Patel, S. Judex, B. Sitharaman, Fabrication and characterization of three-dimensional macroscopic all-carbon scaffolds, Carbon 53 (2013) 90–100.
[10] G. Lalwani, A.M. Henslee, B. Farshid, L. Lin, F.K. Kasper, Y.-X. Qin, A.G. Mikos, B. Sitharaman, Two-dimensional nanostructure-reinforced biodegradable polymeric nanocomposites for bone tissue engineering, Biomacromolecules 14 (2013) 900–909.
[11] J.T. Robinson, F.K. Perkins, E.S. Snow, Z. Wei, P.E. Sheehan, Reduced graphene oxide molecular sensors, Nano Lett. 8 (2008) 3137–3140.
[12] Y. Talukdar, J.T. Rashkow, G. Lalwani, S. Kanakia, B. Sitharaman, The effects of graphene nanostructures on mesenchymal stem cells, Biomaterials 35 (2014) 4863–4877.
[13] S. Park, R.S. Ruoff, Chemical methods for the production of graphenes, Nat. Nanotechnol. 4 (2009) 217–224.
[14] M. Mecklenburg, A. Schuchardt, Y.K. Mishra, S. Kaps, R. Adelung, A. Lotnyk, L. Kienle, K. Schulte, Aerographite: ultra lightweight flexible nanowall, carbon microtube material with outstanding mechanical performance, Adv. Mater. 24 (2012) 3486–3490.
[15] Y.K. Kim, M.H. Kim, D.H. Min, Biocompatible reduced graphene oxide prepared by using dextran as a multifunctional reducing agent, Chem. Commun. 47 (2011) 3195–3197.
[16] E.C. Salas, Z.Z. Sun, A. Luttge, J.M. Tour, Reduction of graphene oxide via bacterial respiration, ACS Nano 4 (2010) 4852–4856.
[17] M.J. Fernandez- Merino, L. Guardia, J.I. Paredes, S. Villar- Rodil, P. Solis-Fernandez, A. Martinez-Alonso, J.M.D. Tascon, Vitamin C is an ideal substitute for hydrazine in the reduction of graphene oxide suspensions, J. Phys. Chem. C 114 (2010) 6426–6432.
[18] G.M. Wang, F. Qian, C. Saltikov, Y.Q. Jiao, Y. Li, Microbial reduction of graphene oxide by *Shewanella*, Nano Res. 4 (2011) 563–570.
[19] O. Akhavan, E. Ghaderi, *Escherichia coli* bacteria reduce graphene oxide to bactericidal graphene in a self-limiting manner, Carbon 50 (2012) 1853–1860.
[20] Z.J. Fan, K. Wang, T. Wei, J. Yan, L.P. Song, B. Shao, An environmentally friendly and efficient route for the reduction of graphene oxide by aluminum powder, Carbon 48 (2010) 1686–1689.
[21] C.Z. Zhu, S.J. Guo, Y.X. Fang, S.J. Dong, Reducing sugar: new functional molecules for the green synthesis of graphene nanosheets, ACS Nano 4 (2010) 2429–2437.
[22] S.S. Chen, W.W. Cai, R.D. Piner, J.W. Suk, Y.P. Wu, Y.J. Ren, J.Y. Kang, R.S. Ruoff, Synthesis and characterization of large-area graphene and graphite films on commercial Cu-Ni alloy foils, Nano Lett. 11 (2011) 3519–3525.
[23] Y. Wang, Z.X. Shi, J. Yin, Facile synthesis of soluble graphene via a green reduction of graphene oxide in tea solution and its biocomposites, ACS Appl. Mater. Interfaces 3 (2011) 1127–1133.
[24] S. Gurunathan, J.W. Han, V. Eppakayala, J.H. Kim, Microbial reduction of graphene oxide by *Escherichia coli*: a green chemistry approach, Colloids Surf. B-Biointerfaces 102 (2013) 772–777.
[25] Y. Tanizawa, Y. Okamoto, K. Tsuzuki, Y. Nagao, N. Yoshida, R. Tero, S. Iwasa, A. Hiraishi, Y. Suda, H. Takikawa, R. Numano, H. Okada, R. Ishikawa, A. Sandhu, Microorganism mediated synthesis of reduced graphene oxide films, Asia-Pacific Interdisciplinary Research Conference 2011 (Ap-Irc 2011) 352 (2012).
[26] M. Baalousha, F.V.D. Kammer, M. Motelica- Heino, P. Le Coustumer, Natural sample fractionation by F1FFF-MALLS-TEM: sample stabilization, preparation, pre- concentration and fractionation, J. Chr. A. 1093 (2005) 156–166.
[27] T. Hofmann, F. von der Kammer, Estimating the relevance of engineered carbonaceous nanoparticle facilitated transport of hydrophobic organic contaminants in porous media, Environ. Poll. 157 (2009) 1117–1126.
[28] N.R. Krieg, Bacterial classification—an overview, Can. J. Microbiol. 34 (1988) 536–540.
[29] P. Saha, S. Krishnamurthi, A. Bhattacharya, R. Sharma, T. Chakrabarti, *Fontibacillus aquaticus* gen. nov. sp. nov., isolated from a warm spring, Int. J. Sys. Evol. Microbiol. 60 (2009) 422–428.
[30] T. Szabo, O. Berkesi, P. Forgo, K. Josepovits, Y. Sanakis, D. Petridis, I. Dekany, Evolution of surface functional groups in a series of progressively oxidized graphite oxides, Chem. Mater. 18 (2006) 2740–2749.
[31] C.D. Zangmeister, Preparation and evaluation of graphite oxide reduced at 220 °C, Chem. Mat. 22 (2010) 5625–5629.
[32] B.L. Allen, P.D. Kichambare, P. Gou, I.I. Vlasova, A.A. Kapralov, N. Konduru, V.E. Kagan, A. Star, Biodegradation of single-walled carbon nanotubes through enzymatic catalysis, Nano Lett. 8 (2008) 3899–3903.
[33] B.L. Allen, G.P. Kotchey, Y. Chen, N.V.K. Yanamala, J. Klein- Seetharaman, V.E. Kagan, A. Star, Mechanistic investigations of horseradish

peroxidase-catalyzed degradation of single-walled carbon nanotubes, J. Am. Chem. Soc. 131 (2009) 17194–17205.
[34] V.E. Kagan, N.V. Konduru, W. Feng, B.L. Allen, J. Conroy, Y. Volkov, I.I. Vlasova, N.A. Belikova, N. Yanamala, A. Kapralov, Y.Y. Tyurina, J. Shi, E.R. Kisin, A.R. Murray, J. Franks, D. Stolz, P. Gou, J. Klein-Seetharaman, B. Fadeel, A. Star, A.A. Shvedova, Carbon nanotubes degraded by neutrophil myeloperoxidase induce less pulmonary inflammation, Nat. Nanotech. 5 (2010) 354–359.
[35] X. Liu, R.H. Hurt, A.B. Kane, Biodurability of single-walled carbon nanotubes depends on surface functionalization, Carbon 48 (2010) 1961–1969.
[36] W. Xing, G. Lalwani, I. Rusakova, B. Sitharaman, Degradation of graphene by hydrogen peroxide, Part. Part. Syst. Charact. 31 (2014) 745–750.
[37] H.T. Liu, L. Zhang, Y.L. Guo, C. Cheng, L.J. Yang, L. Jiang, G. Yu, W.P. Hu, Y.Q. Liu, D.B. Zhu, Reduction of graphene oxide to highly conductive graphene by Lawesson's reagent and its electrical applications, J. Mat. Chem. C 1 (2013) 3104–3109.
[38] P. Khanra, T. Kuila, N.H. Kim, S.H. Bae, D.S. Yu, J.H. Lee, Simultaneous bio-functionalization and reduction of graphene oxide by baker's yeast, Chem. Eng. J. 183 (2012) 526–533.
[39] L.Q. Xu, W.J. Yang, K.G. Neoh, E.T. Kang, G.D. Fu, Dopamine-induced reduction and functionalization of graphene oxide nanosheets, Macromolecules 43 (2010) 8336–8339.
[40] Y. Zhou, Q.L. Bao, L.A.L. Tang, Y.L. Zhong, K.P. Loh, Hydrothermal dehydration for the green reduction of exfoliated graphene oxide to graphene and demonstration of tunable optical limiting properties, Chem. Mater. 21 (2009) 2950–2956.
[41] J.L. Zhang, H.J. Yang, G.X. Shen, P. Cheng, J.Y. Zhang, S.W. Guo, Reduction of graphene oxide via L-ascorbic acid, Chem. Commun. 46 (2010) 1112–1114.
[42] T.A. Pham, J.S. Kim, J.S. Kim, Y.T. Jeong, One-step reduction of graphene oxide with L-glutathione, Colloids Surf. A-Phys. Eng. Asp. 384 (2011) 543–548.
[43] G.X. Wang, J. Yang, J. Park, X.L. Gou, B. Wang, H. Liu, J. Yao, Facile synthesis and characterization of graphene nanosheets, J. Phy. Chem. C 112 (2008) 8192–8195.
[44] M.A. Pimenta, G. Dresselhaus, M.S. Dresselhaus, L.G. Cancado, A. Jorio, R. Saito, Studying disorder in graphite-based systems by Raman spectroscopy, Phys. Chem. Chem. Phys. 9 (2007) 1276–1291.
[45] H.A. Becerril, J. Mao, Z. Liu, R.M. Stoltenberg, Z. Bao, Y. Chen, Evaluation of solution-processed reduced graphene oxide films as transparent conductors, ACS Nano 2 (2008) 463–470.
[46] G. Eda, G. Fanchini, M. Chhowalla, Large-area ultrathin films of reduced graphene oxide as a transparent and flexible electronic material, Nat. Nanotechnol. 3 (2008) 270–274.
[47] M. Fu, Q.Z. Jiao, Y. Zhao, H.S. Li, Vapor diffusion synthesis of CoFe2O4 hollow sphere/graphene composites as absorbing materials, J. Mat. Chem. A 2 (2014) 735–744.